Submesoscale potential vorticity

Journal:	*Journal of Fluid Mechanics*
Manuscript ID	JFM-21-1376
Manuscript Type:	JFM Papers
Date Submitted by the Author:	19-Aug-2021
Complete List of Authors:	Buckingham, Christian; Université de Bretagne Occidentale,
JFM Keywords:	Baroclinic flows < Geophysical and Geological Flows, Rotating flows < Geophysical and Geological Flows, Stratified flows < Geophysical and Geological Flows
Abstract:	Ertel's potential vorticity theorem is essentially a clever combination of two conservation principles. The result is a conserved scalar q that accurately reflects vorticity values that fluid parcels can possess and acts as a tracer for fluid flow. While true at large horizontal scales in the ocean and atmosphere, at increasingly smaller scales and in sharply curved fronts, its accuracy breaks down. This is because Earth's rotation imparts angular momentum to fluid parcels and the conservation of absolute angular momentum L restricts the range of centripetal accelerations possible in balanced flow; this correspondingly restricts vorticity. To address this discrepancy, we revisit Ertel's derivation and obtain a new conserved scalar Lq that more properly reflects the vorticity of fluid parcels at these small horizontal scales. Although limited to flows on the f plane, this theorem nevertheless highlights a fundamental principle applicable to all geophysical fluids: at sufficiently small horizontal scales such that L can appropriately be defined, centripetal accelerations—or curvature—can modify the vorticity of fluid parcels observed on the sphere.

Under consideration for publication in J. Fluid Mech.

Submesoscale potential vorticity

Christian E. Buckingham[1] †

[1]Université de Bretagne Occidentale, CNRS, IRD, Ifremer, Laboratoire d'Océanographie Physique et Spatiale, IUEM, Rue Dumont d'Urville, 29280, Plouzané, FR

[2]British Antarctic Survey, Cambridge, CB3 0ET, UK

(Received xx; revised xx; accepted xx)

Ertel's potential vorticity theorem is essentially a clever combination of two conservation principles. The result is a conserved scalar q that accurately reflects vorticity values that fluid parcels can possess and acts as a tracer for fluid flow. While true at large horizontal scales in the ocean and atmosphere, at increasingly smaller scales and in sharply curved fronts, its accuracy breaks down. This is because Earth's rotation imparts angular momentum to fluid parcels and the conservation of absolute angular momentum L restricts the range of centripetal accelerations possible in balanced flow; this correspondingly restricts vorticity. To address this discrepancy, we revisit Ertel's derivation and obtain a new conserved scalar Lq that more properly reflects the vorticity of fluid parcels at these small horizontal scales. Although limited to flows on the f plane, this theorem nevertheless highlights a fundamental principle applicable to all geophysical fluids: at sufficiently small horizontal scales such that L can appropriately be defined, centripetal accelerations–or curvature–can modify the vorticity of fluid parcels observed on the sphere.

Key words: These will be chosen by the author during the online submission process and will then be added during the typesetting process (see Keyword PDF for the full list). Other classifications will be added at the same time.

MSC Codes *(Optional)*

1. Introduction

Ocean dynamics at small horizontal scales have garnered considerable attention in recent years. This attention has been evident in both *observational* and *modelling* sectors of the physical oceanographic community. New advancements in observing systems–including those from autonomous floats (D'Asaro *et al.* 2011), gliders (Thompson *et al.* 2016; du Plessis *et al.* 2019), and long-range surface vehicles such as SailDrones (Gentemann *et al.* 2020)–have increased our capability to resolve small-scale phenomena. One result is that gradients in velocity and density at horizontal scales between 1 and 10 km–previously only inferred

† Email address for correspondence: christian.buckingham@gmail.com

from spacecraft (*e.g.* Flament *et al.* 1985; Scully-Power 1986; Munk *et al.* 2000) and long-term moored measurements (*e.g.* Bane *et al.* 1989; Lilly & Rhines 2002; Buckingham *et al.* 2016)–are now resolved or becoming resolved in targeted process studies (*e.g.* Thomas & Lee 2005; D'Asaro *et al.* 2011; Shcherbina *et al.* 2013; Thomas *et al.* 2013; Adams *et al.* 2017; Naveira Garabato *et al.* 2019). At the same time, computational resources have increased at an unimaginable rate, permitting scientists the ability to realistically simulate dynamics at such fine scales in numerical models. At present, models are capable of providing realistic ocean simulations within nested, regional configurations, horizontal grid resolutions of 100 m are possible (Onken *et al.* 2020), with the result that oceanic phenomena with e-folding scales of several hundred meters can be resolved. These same simulations run on the globe produce simulations at horizontal resolutions approaching 1 km (https://data.nas.nasa.gov/ecco/data.php).

Oceanic flows at these small spatial scales are commonly referred to as *submesoscale processes* (Thomas *et al.* 2008; McWilliams 2016) in order to distinguish them from larger-scale counter-parts, referred to as *mesoscale processes*. At mid-latitudes, these terms correspond to horizontal scales smaller than 10 km (submesoscale) and larger than 30 km (mesoscale), where the transition between these scales is roughly equal to the first-mode, baroclinic deformation radius R_d (Chelton *et al.* 1998; Smith 2007). It is notable that at high latitudes, R_d approaches 1-10 km (Timmermans *et al.* 2008; Nurser & Bacon 2014) such that assigning absolute scales to these phenomena is problematic. This has motivated a dynamical definition (Thomas *et al.* 2008; McWilliams 2016).

1.1. *A dynamical definition of the oceanic submesoscale*

Processes within the oceanic submesoscale regime are typically characterized by enhanced gradients in velocity and density. In particular, the vertical component of relative vorticity $\zeta = (\nabla \times \boldsymbol{u}) \cdot \hat{\boldsymbol{k}}$ rivals the vertical component of planetary vorticity $f = 2\boldsymbol{\Omega} \cdot \hat{\boldsymbol{k}} = 2\Omega \sin\theta$ and, as a consequence of thermal wind balance (TWB), $\partial_z \boldsymbol{u}_h = \frac{1}{f} \hat{\boldsymbol{k}} \times \nabla_h b$, pronounced horizontal density gradients imply enhanced vertical shears. Finally, mixing is typically enhanced within boundary layers, such that vertical stratification N^2 is reduced. As a consequence, both gradient Rossby number ($Ro = \zeta/f$) and gradient Richardson number ($Ri = N^2/|\partial_z \boldsymbol{u}_h|^2$) have values which approach 1.0 within the oceanic submesoscale regime (Thomas *et al.* 2008; McWilliams 2016).

1.2. *Broadening this definition to accommodate vortex flow*

It is common to assume that the mean flow within fronts is in geostrophic and hydrostatic balance–*i.e.* TWB mentioned above. In Cartesian coordinates oriented relative to the front, we can write this as $f\partial_z \overline{v} = \partial_x \overline{b}$, where $M^2 = \partial_x \overline{b}$ denotes the mean cross-frontal buoyancy gradient. In these expressions, $\boldsymbol{u_h}$ is the horizontal velocity, $\overline{v}$ denotes the mean velocity in the along-front direction, $\partial_z \overline{v}$ is the mean vertical shear, $b = -g\rho/\rho_o$ denotes buoyancy (g is gravity, ρ is density, and ρ_o is a reference density), and x and y are cross-front and along-front coordinates, respectively. This is a reasonable approximation for density fronts with horizontal scales larger than R_d (Pedlosky 1987). However, at increasingly smaller scales, the momentum balance can shift from a geostrophic to cyclogeostrophic balance, reflecting the growing importance of centripetal accelerations. Together with the hydrostatic balance, this implies a gradient wind balance (GWB):

$$(f + 2\overline{v}/r)\partial_z \overline{v} = \partial_r \overline{b} \tag{1.1}$$

Factoring out the Coriolis parameter from the quantity in parentheses immediately leads to a nondimensional parameter which quantifies the impact of centripetal accelerations on

the vertical shear, the curvature number: $Cu = 2\overline{v}/(fr)$. This nondimensional number also scales with the ratio of centripetal to Coriolis accelerations (Shakespeare 2016). In the expression above, r denotes the cross-front coordinate, such that $M^2 = \partial_r \overline{b}$ is the radial gradient buoyancy gradient and implicitly contains information regarding frontal curvature. For clarity, note that $Cu > 0$ for cyclonic curved fronts and $Cu < 0$ negative for anticyclonic curved fronts. (In vortices, r is the distance from the vortex center, while $\overline{v} > 0$ for cyclones and $\overline{v} < 0$ for anticyclones. In meandering baroclinic frontal flows, we can replace r with a local radius of curvature R. Since the along-front flow is $\overline{v} > 0$, R must be signed.) Moreover, in the limit $Cu \to 0$ one recovers TWB. GWB is therefore descriptive of highly curved fronts and vortices and includes TWB as a limiting case. We therefore broaden the definition of the oceanic submesoscale as being a regime in which the mean flow is in GWB, and where gradient Rossby, Richardson, and curvature numbers (Ro, Ri, Cu) can be of order-one.

1.3. *Observations of relative vorticity at kilometer-scales*

It is broadly understood that the distribution of relative vorticity as measured at submesoscale (*i.e.* 1-10 km) resolutions in the oceans has two limiting characteristics. First, the distribution of Ro is predominantly cyclonic (positively skewed) for frontal flows and predominantly anticyclonic (negatively skewed) for eddying or vortex flows (Figure 1). By "vortex flow," we include both highly curved fronts and coherent vortices. This has been noted, for example, in the upper ocean observations (Rudnick 2001; Shcherbina *et al.* 2013; Buckingham *et al.* 2016) and model simulations (Roullet & Klein 2010; Shcherbina *et al.* 2013). Away from the upper ocean, the cyclone-anticyclone asymmetry has been documented in float trajectories, vertical hydrographic profiles, and moored measurements (*e.g.* McDowell & Rossby 1978; Riser *et al.* 1986; D'Asaro 1988; Bane *et al.* 1989; Zhao *et al.* 2014), but here the statistics are more limited.

To aid in our discussions, we reproduce in Figure 1 the joint probability density function (PDF) of vorticity ζ and strain rate $\alpha = [(\partial_x u - \partial_y v)^2 + (\partial_x v + \partial_y u)^2]^{1/2}$ as documented by (Shcherbina *et al.* 2013, Figure 5). As vorticity increases, the joint PDF approaches a pure shear relationship and is unbounded ($\zeta \approx \alpha$), indicative of fronts. By contrast, as vorticity decreases (becomes more negative), the negative vorticity is bounded, with a higher probability of solid-body rotation ($\zeta \gg \alpha$), indicative of vortex flow. While the unbounded nature of cyclonic vorticity associated with straight fronts can be rationalized in terms of potential vorticity (PV) conservation (Hoskins & Bretherton 1972)†, the increased likelihood of anticyclonic vorticity associated with vortex flow has not fully been explained. In this study, we provide an explanation for this characteristic.

1.4. *Motivation and outline of the study*

In a previous study (Buckingham *et al.* 2020*a*,*b*), it was suggested that a unique conservation principle may be present within highly curved fronts and vortices (hereafter "vortex flow") on the f-plane. Moreover, this principle was invoked when proposing a mechanism for the evolution of small-scale (*i.e.* submesoscale and polar mesoscale) vortices in the ocean. The implication was that fluid parcels within curved baroclinic fronts and vortices do not simply conserve the Ertel PV (Ertel 1942), and therefore undergo vortex stretching and tilting to

† It helps to think of this in the barotropic limit, for which the equation for the evolution of vorticity is $D\zeta/Dt = (f + \zeta)\partial_z w - \beta v$, where v is meridional velocity, w is vertical velocity, and $\beta = df/dy$. Letting $\beta = 0$, dynamically, what occurs is that as a fluid parcel is stretched ($\partial_z w > 0$), it spins up cyclonically without bound. As this same fluid parcel is compressed ($\partial_z w < 0$), it spins in an opposite direction. However, this motion is bounded since $D\zeta/Dt$ becomes increasingly smaller as ζ approaches $-f$. In non-dimensional form, we find that $Ro > -1$. In the baroclinic limit, other constraints (*i.e.* on density) become important and modify this lower bound. In particular, the bound is $Ro > -1 + Ri^{-1}$.

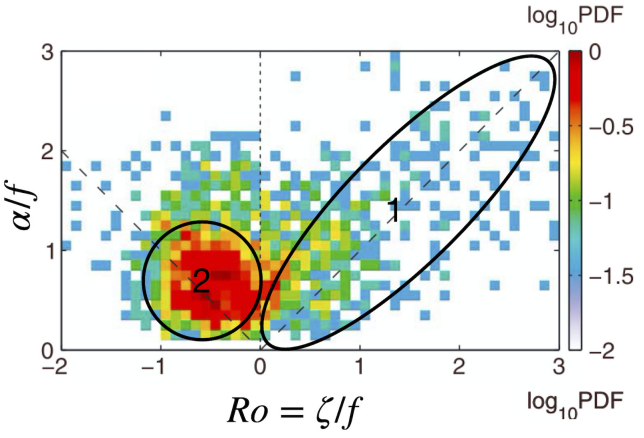

Figure 1: The joint PDF of relative vorticity ζ and magnitude strain rate α normalized by the Coriolis parameter f as documented in observations in the vicinity of the Gulf Stream; adapted from Shcherbina *et al.* (2013, Figure 5a). Two regimes are identified: (1) cyclonic vorticity that approaches the strain rate α with increasing vorticity (indicative of straight fronts) and (2) anticyclonic vorticity that is bounded in $Ro = \zeta/f$ (indicative of vortex flow). The unbounded nature of cyclonic vorticity can be explained using PV conservation at a geostrophic front, while the peak associated with anticyclonic vortex flow can be explained using Lq conservation.

conserve this quantity. Rather, fluid parcels adjust barotropic and baroclinic components of another scalar,‡ which is proportional to the product of the Ertel PV (q) and the vertical component of absolute angular momentum (L). If true, the fact that this additional term L enters the conserved quantity provides an added constraint to the problem, making inviscid, adiabatic motions within highly curved baroclinic flows differ from those in which PV alone is the conserved scalar. As is demonstrated below, this places constraints on relative vorticity and may help to explain the characteristic of vorticity just described (cf. Figure 1). A key assumption is continuity of the fluid in the direction of the mean flow at radius r such that L can be appropriately defined (Rayleigh 1917; Shakespeare 2016). In the oceans, at scales dynamically described as "submesoscale" (*e.g.* horizontal scales 1-10 km) this is possible.

The purpose of this manuscript is three-fold. First, we wish to provide a rational argument for the statement that "the product of the absolute angular momentum and Ertel PV is conserved following fluid parcels." Second, we wish to assess under which conditions such a statement is true. Third, we seek to fully explain above feature within the distributions of relative vorticity. In doing so, we indirectly lay a more formal foundation for the analysis of flows in which centrifugal forces are present.

The outline of the study is as follows. We first derive a conservation equation for the new scalar quantity Lq (section 2). This derivation follows that of Ertel (1942) but includes a presentation of absolute angular momentum, a topic neglected in most oceanographic studies. Application of the theorem to oceanic flows is discussed in section 3 and its limitations are described in section 4. The study concludes in section 5.

‡ Buckingham *et al.* (2020*a*,*b*) suggested that the generalized Rayleigh discriminant $\Phi = 2Lq/r^2$ was conserved following fluid parcels in highly curved fronts and vortices. However, as demonstrated below, this statement is incorrect: it is Lq or $r^2\Phi$ that is conserved following fluid parcels. This difference is critical because it implies cross-frontal motion will modify the stability "seen" by fluid parcels.

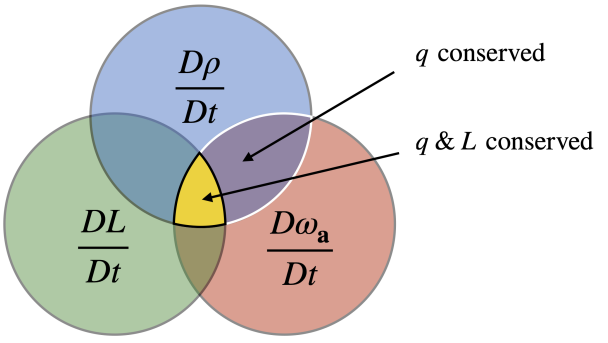

Figure 2: A Venn diagram conceptually depicting the intersection of three conservation principles: absolute vorticity $\boldsymbol{\omega_a}$, density ρ, and the vertical component of absolute angular momentum L. Ertel (1942) focused on the intersection of density and vorticity conservation. This study examines a subset of such flows for which both PV q and absolute angular momentum L can be conserved (*i.e.* vortex flow).

2. Derivation

Ertel's (1942) PV theorem is a clever combination of two independent conservation principles, each with its conditions. It is therefore logical to presume that the inclusion of a third conservation principle together with its corresponding conditions could permit a new vorticity theorem subject to these additional limitations. This is illustrated conceptually in Figure 2.

2.1. *Governing equations*

The equations of motion describing the balance of forces per unit mass of a fluid parcel within a rotating reference frame are (Batchelor 1967; Pedlosky 1987; Cushman-Roisin 1994)

$$\frac{D\boldsymbol{u}}{Dt} + 2\boldsymbol{\Omega}\times\boldsymbol{u} = -\frac{1}{\rho}\nabla p + \underbrace{\boldsymbol{g}^* + \boldsymbol{a_c}}_{\boldsymbol{g}} + \frac{\mathscr{F}}{\rho}, \tag{2.1}$$

where it is understood that all terms are evaluated within the rotating reference frame. Here, $D/Dt = \partial_t + \boldsymbol{u}\cdot\nabla\boldsymbol{u}$ denotes the material or substantial derivative, $\boldsymbol{r}$ is the position vector, $\boldsymbol{\Omega}$ is the angular rotation rate ($|\boldsymbol{\Omega}| = 2\pi/\text{day} \approx 7.22\times10^{-5}$ s^{-1} for Earth) and assumed to be constant, $2\boldsymbol{\Omega}\times\boldsymbol{u}$ is the Coriolis acceleration, $\boldsymbol{a_c} = -\boldsymbol{\Omega}\times(\boldsymbol{\Omega}\times\boldsymbol{r}) = |\boldsymbol{\Omega}|^2\boldsymbol{r}_\perp$ is the centrifugal acceleration due to the rotation of the reference frame, ρ is density, p is pressure, $\boldsymbol{g}^*$ is the acceleration due to gravity, and $\mathscr{F}$ denotes the frictional force. It is customary to combine centrifugal and gravitational accelerations into a resultant acceleration $\boldsymbol{g} = \boldsymbol{g}^* + \boldsymbol{a_c}$, or *effective gravity*. The resultant is then approximately perpendicular to geopotential surfaces and, hence, oriented vertically† (Cushman-Roisin 1994). For clarity, we illustrate planetary vorticity, gravitational acceleration, gravity, and centrifugal acceleration vectors (Figure 3).

Mass conservation is given by the continuity equation

$$\frac{\partial\rho}{\partial t} + \boldsymbol{\nabla}\cdot(\rho\boldsymbol{u}) = 0. \tag{2.2}$$

An equation of state is typically necessary to relate ρ to known or measured variables. In the ocean, this is a complex function of temperature, salinity, and pressure. For simplicity in the present work, we assume we know the density perfectly.

† Local changes to the gravitational potential, for example, due to irregular topography or seamounts, will perturb $\boldsymbol{g}^*$ from its mean direction.

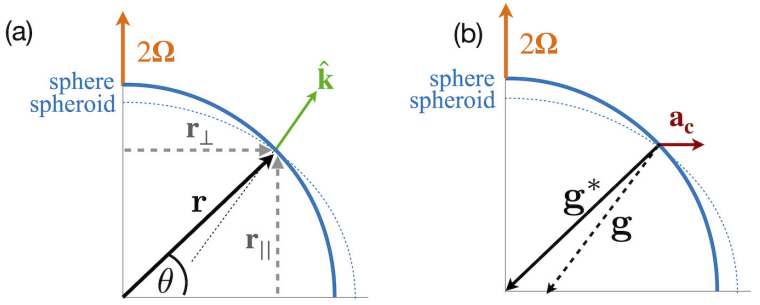

Figure 3: Illustration of vectors present within the equations of motion on the sphere (cf. Equation 2.1) and f-plane approximation (cf. Equation 2.3). In (a), we depict planetary vorticity $2\boldsymbol{\Omega}$ (orange), the position vector $\boldsymbol{r}$ (heavy black), components of the position vector $\boldsymbol{r}_\perp$ and $\boldsymbol{r}_{||}$ (gray), and vertical unit vector $\hat{\boldsymbol{k}}$ (green). In (b), we depict the gravitational vector $\boldsymbol{g}^*$ (black), the centrifugal acceleration vector $\boldsymbol{a_c} = -\boldsymbol{\Omega} \times (\boldsymbol{\Omega} \times \boldsymbol{r}) = |\boldsymbol{\Omega}|^2 \boldsymbol{r}_\perp$ (red), and the vector resultant, or effective gravity $\boldsymbol{g} = \boldsymbol{g}^* + \boldsymbol{a_c}$ (dashed black). We also illustrate the surface of Earth as represented by a sphere (solid blue) and oblate spheroid (dashed blue). The unit vector $\hat{\boldsymbol{k}}$ is anti-parallel to $\boldsymbol{g}$ and, therefore, approximately perpendicular to the surface of the oblate spheroid.

The f-plane approximation: rational and self-consistent

The corresponding equations of motion valid under the f plane approximation are obtained by expressing Equation 2.1 in spherical coordinates, scaling the equations of motion, and discarding terms multiplied by $\delta = |ds|/R_e \ll 1$ or smaller, where $|ds| = R_e d\theta$ denotes a meridional arc length and R_e is the mean radius of Earth (Grimshaw 1975). The result is a vectorized set of equations comparable to Equation 2.1 except where $2\boldsymbol{\Omega} \times \boldsymbol{u}$ is evaluated at a specific latitude θ_o:

$$\frac{D\boldsymbol{u}}{Dt} + 2\boldsymbol{\Omega_o} \times \boldsymbol{u} = -\frac{1}{\rho}\nabla p + \boldsymbol{g} + \frac{\mathscr{F}}{\rho}. \tag{2.3}$$

In the cylindrical coordinate system, where the triad of orthogonal unit vectors $(\hat{\boldsymbol{r}}, \hat{\boldsymbol{\phi}}, \hat{\boldsymbol{k}})$ point in radial, azimuthal, and vertical (upward) directions, respectively, the position vector is denoted by $\boldsymbol{r_c} = (r, \phi, z)$ and velocity by $\boldsymbol{u} = (u, v, w)$ (Figure 4). The material derivative is then $D/Dt = \partial_t + \boldsymbol{u} \cdot \nabla = \partial_t + u\partial_r + (v/r)\partial_\phi + w\partial_z$. Finally, the frictional force is $\mathscr{F} = (F_r, F_\phi, F_z)$ and effective gravity is $\boldsymbol{g} = (0, 0, -g)$. The choice of a cylindrical coordinate system on the f plane slightly complicates expression of planetary vorticity $2\boldsymbol{\Omega_o}$ owing to its variation with azimuth angle ϕ. Defining ϕ with respect to east, we have $2\boldsymbol{\Omega_o} = (0, 2|\boldsymbol{\Omega}| \cos\theta_o \sin\phi, 2|\boldsymbol{\Omega}| \sin\theta_o) = (0, \tilde{f}, f)$. To retain generality in our derivation below, we use Equation 2.3 together with the full Coriolis vector $\boldsymbol{\Omega_o}$. Note, Equation 2.2 remains unaltered under the f plane approximation. Additionally, the position vectors in the spherical and cylindrical coordinate systems are related by $\boldsymbol{r} = \boldsymbol{r_o} + \boldsymbol{r_c}$, where $\boldsymbol{r_o}$ denotes the origin of the cylindrical system at latitude θ_o(Figure 4).

Equation 2.3 is rational in that it follows logically from the spherical equations in the limit of small arc length. Moreover, as pointed out by Grimshaw (1975), the equation is also *self-consistent*; it possesses certain mathematical properties–*e.g.* differentiation is commutative–that permit subsequent derivations of vorticity, Ertel's PV theorem, etc. to be equivalent to those in spherical coordinates subject to these limiting conditions. This self-consistency is an important aspect of the derivation as it enables us to write a conservation equation for the absolute angular momentum that properly reflects dynamics on the oblate sphere. In contrast,

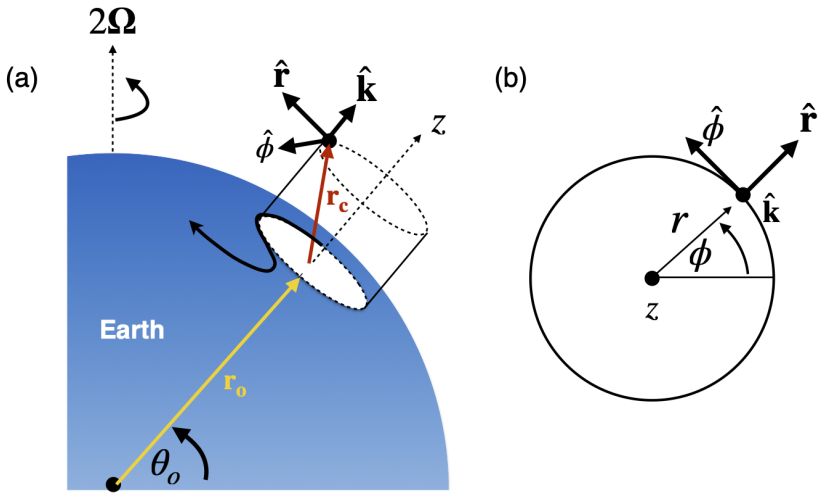

Figure 4: A cylindrical coordinate system on an f-plane at latitude $\theta = \theta_o$: (a) perspective view and (b) plan view, illustrating the orthogonal unit basis $(\hat{\boldsymbol{r}}, \hat{\boldsymbol{\phi}}, \hat{\boldsymbol{k}})$, position vector $\boldsymbol{r_c} = (r, \phi, z)$ (red), where the angle ϕ is defined relative to an eastward direction, and a vector $\boldsymbol{r_o}$ (yellow) which helps define the origin of the cylindrical coordinate system. Although not shown, the velocity is $\boldsymbol{u} = (u, v, w)$ and its components point in $\hat{\boldsymbol{r}}$, $\hat{\boldsymbol{\phi}}$, and $\hat{\boldsymbol{k}}$ directions, respectively.

the equations of motion under the β-plane approximation are not self-consistent (Grimshaw 1975) and may introduce dynamics not encountered on the sphere.

2.2. *Absolute vorticity*

Starting with the equations of motion, one can derive a conservation equation for absolute vorticity (Batchelor 1967; Pedlosky 1987; Müller 1995). We first re-express Equation 2.3 in terms of absolute vorticity $\boldsymbol{\omega_a} = \nabla \times \boldsymbol{u_a} = 2\boldsymbol{\Omega_o} + \nabla \times \boldsymbol{u} = 2\boldsymbol{\Omega_o} + \boldsymbol{\omega}$ (Batchelor 1967):

$$\frac{\partial \boldsymbol{u}}{\partial t} + \boldsymbol{\omega_a} \times \boldsymbol{u} = -\frac{1}{\rho}\nabla p + \nabla\left[\boldsymbol{g} \cdot \boldsymbol{r_c} - (\boldsymbol{u} \cdot \boldsymbol{u})/2\right] + \frac{\mathscr{F}}{\rho}, \tag{2.4}$$

where $\boldsymbol{u_a} = \boldsymbol{u} + \boldsymbol{\Omega} \times \boldsymbol{r_c}$ is absolute velocity. Taking the curl of Equation 2.4 gives

$$\frac{\partial \boldsymbol{\omega}}{\partial t} + \nabla \times (\boldsymbol{\omega_a} \times \boldsymbol{u}) = \frac{\nabla\rho \times \nabla p}{\rho^2} + \nabla \times \left(\frac{\mathscr{F}}{\rho}\right). \tag{2.5}$$

Using $\nabla \times (\boldsymbol{A} \times \boldsymbol{B}) = \boldsymbol{A}\nabla \cdot \boldsymbol{B} + (\boldsymbol{B} \cdot \nabla)\boldsymbol{A} - \boldsymbol{B}\nabla \cdot \boldsymbol{A} - (\boldsymbol{A} \cdot \nabla)\boldsymbol{B}$ (*e.g.* Riley *et al.* 2006), noting that the planetary vorticity is constant,†, and using the continuity equation (cf. Equation 2.2), we obtain a conservation equation for the absolute vorticity *per unit mass*:

$$\frac{D}{Dt}\left(\frac{\boldsymbol{\omega_a}}{\rho}\right) = \left(\frac{\boldsymbol{\omega_a}}{\rho} \cdot \nabla\right)\boldsymbol{u} + \frac{\nabla\rho \times \nabla p}{\rho^3} + \left(\nabla \times \frac{\mathscr{F}}{\rho}\right)\frac{1}{\rho}. \tag{2.6}$$

Here, the divergence term $\omega_a \boldsymbol{\nabla} \cdot \boldsymbol{u}$ has been eliminated from the right-hand-side (RHS) by including density within the material derivative on the left-hand-side (LHS).

† This is true regardless of the chosen coordinate system since, ignoring the precession of Earth's rotation axis, the vector $\boldsymbol{2\Omega}$ is unchanged.

2.3. *Density or buoyancy (i.e. a thermodynamic variable)*

Here, we follow Pedlosky (1987) (Ertel assumes $D\rho/Dt = 0$) and write the conservation of a scalar λ as

$$D\lambda/Dt = \frac{\partial \lambda}{\partial t} + \boldsymbol{u} \cdot \nabla \lambda = \Psi. \tag{2.7}$$

Taking the inner product of $\nabla\lambda$ and Equation 2.6, one obtains

$$\nabla\lambda \cdot \frac{D}{Dt}\left(\frac{\boldsymbol{\omega_a}}{\rho}\right) = \nabla\lambda \cdot \left[\left(\frac{\boldsymbol{\omega_a}}{\rho} \cdot \nabla\right)\boldsymbol{u}\right] + \nabla\lambda \cdot \frac{\nabla\rho \times \nabla p}{\rho^3} + \frac{\nabla\lambda}{\rho} \cdot \left(\nabla \times \frac{\mathscr{F}}{\rho}\right). \tag{2.8}$$

Incorporating $\nabla\lambda$ into the material derivative on the LHS,† we obtain

$$\frac{Dq}{Dt} = \frac{D}{Dt}\left(\frac{\boldsymbol{\omega_a}}{\rho} \cdot \nabla\lambda\right) = \frac{\boldsymbol{\omega_a}}{\rho} \cdot \nabla\Psi + \nabla\lambda \cdot \frac{\nabla\rho \times \nabla p}{\rho^3} + \frac{\nabla\lambda}{\rho} \cdot \left(\nabla \times \frac{\mathscr{F}}{\rho}\right). \tag{2.9}$$

Choosing, for example, density (or a quantity proportional to density) as our scalar $\lambda = \rho$, while requiring frictional and diabatic processes to be zero so that the flow is inviscid and density is conserved, we see that all three terms on the RHS vanish and $q = (\boldsymbol{\omega_a}/\rho) \cdot \nabla\lambda$ is conserved following fluid parcels. This is Ertel's PV theorem.

2.4. *Absolute angular momentum*

One of the contributions of Rayleigh (1917) was to demonstrate that, if a vortex is axisymmetric (*i.e.* $\partial/\partial\phi = 0$), then the azimuthal momentum equation can be multiplied by r and re-expressed as a conservation equation for the angular momentum per unit mass: $D/Dt(r\overline{v}) = 0$, where $\overline{v}$ denotes the azimuthal velocity. Application of this approach to a fluid parcel in a rotating reference frame with constant rotation rate also permits such a rearrangement: $DL/Dt = 0$, where $L = r\overline{v} + fr^2/2$ is now the *absolute angular momentum*, and is the sum of relative angular momentum ($r\overline{v}$) and planetary angular momentum imparted by the rotating reference frame. Importantly, the absolute angular momentum of a fluid parcel in a vortex on the f-plane *is exactly the same as if the vortex were located at the center of the rotating reference frame*, where r is the magnitude of the position vector (Kloosterziel & van Heijst 1991). **This motivates the following vector representation.**

We orient our coordinate system so that its origin is at the center of a curved front or vortex (cf. Figure 4). Taking the cross product of the position vector $\boldsymbol{r_c}$ and each of the terms in Equation 2.3, one obtains after some effort

$$\frac{D\boldsymbol{m_a}}{Dt} = -\boldsymbol{\Omega_o} \times \boldsymbol{m} - \frac{\boldsymbol{r_c} \times \nabla p}{\rho} + \boldsymbol{r_c} \times \boldsymbol{g} + \frac{\boldsymbol{r_c} \times \mathscr{F}}{\rho}, \tag{2.10}$$

where $\boldsymbol{m_a} = \boldsymbol{r_c} \times \boldsymbol{u_a}$ and $\boldsymbol{m} = \boldsymbol{r_c} \times \boldsymbol{u}$ are absolute and relative angular momentum, respectively. Using the definition of absolute velocity, $\boldsymbol{u_a} = \boldsymbol{u} + \boldsymbol{\Omega_o} \times \boldsymbol{r_c}$, we observe that $\boldsymbol{m_a} = \boldsymbol{m} + \boldsymbol{m_\Omega}$ is the sum of relative angular momentum $\boldsymbol{m} = \boldsymbol{r_c} \times \boldsymbol{u}$ and planetary angular momentum $\boldsymbol{m_\Omega} = \boldsymbol{r_c} \times (\boldsymbol{\Omega_o} \times \boldsymbol{r_c})$ in a manner analogous to absolute vorticity $\boldsymbol{\omega_a}$.

For our purposes, we wish to isolate the vertical component of absolute angular momentum. We take the inner product of Equation 2.10 and the vertical unit vector $\hat{\boldsymbol{k}}$ to obtain

$$\frac{DL}{Dt} = -(\boldsymbol{\Omega_o} \times \boldsymbol{m}) \cdot \hat{\boldsymbol{k}} - \frac{\boldsymbol{r_c} \times \nabla p}{\rho} \cdot \hat{\boldsymbol{k}} + (\boldsymbol{r_c} \times \boldsymbol{g}) \cdot \hat{\boldsymbol{k}} + \frac{\boldsymbol{r_c} \times \mathscr{F}}{\rho} \cdot \hat{\boldsymbol{k}}, \tag{2.11}$$

where we have introduced the notation $L = \boldsymbol{m_a} \cdot \hat{\boldsymbol{k}}$ to denote the vertical component of absolute angular momentum, consistent with the literature (Holton 1992; Shakespeare 2016).

† This follows from $\boldsymbol{A} \cdot \frac{D(\nabla\lambda)}{Dt} = \boldsymbol{A} \cdot \nabla\frac{D\lambda}{Dt} - \nabla\lambda \cdot (\boldsymbol{A} \cdot \nabla\boldsymbol{u})$, where $\boldsymbol{A} = \boldsymbol{\omega_a}/\rho$.

Thus, the vertical component of absolute angular momentum L of a fluid parcel is modified by torques due to pressure, gravitation, and friction, as well as a torque produced by Earth's rotation acting on the relative angular momentum $\boldsymbol{m}$. For cases when $\boldsymbol{m}$ is not vertical, the latter reduces L, tilting the absolute angular momentum vector away from the vertical.

A comparison with angular momentum conservation on the spheroid

It is helpful to compare the conservation equation above (cf. Equation 2.10) with that obtained for the oblate sphere (*e.g* Barnes *et al.* 1983; Peixoto & Oort 1992; Bell 1994). In spherical coordinates, the position vector $\boldsymbol{r}$ extends from Earth's center to the fluid parcel (Figure 3). Computing the cross product of $\boldsymbol{r}$ and the more general equations of motion (cf. Equation 2.1) gives (*e.g.* Egger 2001, Equation 2.7)

$$\frac{D\boldsymbol{m_a}}{Dt} = -\boldsymbol{\Omega}\times\boldsymbol{m_a} - \frac{\boldsymbol{r}\times\nabla p}{\rho} + \boldsymbol{r}\times\underbrace{(\boldsymbol{g}-\boldsymbol{a_c})}_{\boldsymbol{g^*}} + \frac{\boldsymbol{r}\times\mathscr{F}}{\rho}, \tag{2.12}$$

where absolute, relative, and planetary angular momentum are now given by $\boldsymbol{m_a} = \boldsymbol{m} + \boldsymbol{m_\Omega}$, $\boldsymbol{m} = \boldsymbol{r}\times\boldsymbol{u}$, and $\boldsymbol{m_\Omega} = \boldsymbol{r}\times(\boldsymbol{\Omega}\times\boldsymbol{r})$, respectively. A useful simplification can now be made. Expanding the first term on the RHS and examining only the planetary portion, we see that Earth's rotation induces a torque with magnitude $|-\boldsymbol{\Omega}\times\boldsymbol{m_\Omega}| = |\boldsymbol{r}_{||}||\boldsymbol{\Omega}||\boldsymbol{\Omega}\times\boldsymbol{r}_\perp| = |\boldsymbol{\Omega}|^2|\boldsymbol{r}_\perp||\boldsymbol{r}_{||}|$ and directed eastward.† Similarly, the torque induced by the centrifugal acceleration has magnitude $|-\boldsymbol{r}\times\boldsymbol{a_c}| = |\boldsymbol{\Omega}|^2|\boldsymbol{r}_\perp||\boldsymbol{r}_{||}|$ and is directed westward. The two terms cancel and Equation 2.12 becomes

$$\frac{D\boldsymbol{m_a}}{Dt} = -\boldsymbol{\Omega}\times\boldsymbol{m} - \frac{\boldsymbol{r}\times\nabla p}{\rho} + \boldsymbol{r}\times\boldsymbol{g} + \frac{\boldsymbol{r}\times\mathscr{F}}{\rho}. \tag{2.13}$$

Therefore, Equation 2.10 is identical to Equation 2.13 is except where $\boldsymbol{r}$ is replaced by $\boldsymbol{r_c}$ and $\boldsymbol{\Omega}$ by $\boldsymbol{\Omega_o}$. This fact follows from the self-consistency of the governing equations on the f plane (Grimshaw 1975). Thus, while a formal proof remains, we argue that absolute angular momentum is conserved on the f plane in the same way that it is conserved on the sphere.‡ This may be why, for sufficiently small horizontal scales and balanced (*i.e.* hydrostatic) flows in which the meridional component of Coriolis is neglected, the volume-integrated, vertical component of absolute angular momentum is approximately conserved (Egger 2001, Fig. 2e).

2.5. *A vorticity theorem for the f plane*

We are now in a position to combine conservation laws (cf. Equations 2.9 and 2.11). It is simple to show that if $\frac{DA}{Dt} = 0$ and if $\frac{DB}{Dt} = 0$, then $\frac{D}{Dt}(AB) = 0$. This is the logic behind the following step. We therefore multiply Equation 2.9 by $L = \boldsymbol{m_a}\cdot\hat{\boldsymbol{k}} = (\boldsymbol{m}+\boldsymbol{m_\Omega})\cdot\hat{\boldsymbol{k}}$ and add this to $q = (\boldsymbol{\omega_a}/\rho)\cdot\nabla\lambda$ multiplied by Equation 2.11. This gives

$$\begin{aligned}\frac{D}{Dt}(Lq) = {} & L\left[\frac{\boldsymbol{\omega_a}}{\rho}\cdot\nabla\Psi + \nabla\lambda\cdot\frac{\nabla\rho\times\nabla p}{\rho^3} + \frac{\nabla\lambda}{\rho}\cdot\left(\nabla\times\frac{\mathscr{F}}{\rho}\right)\right] \\ & + q\left[-(\boldsymbol{\Omega_o}\times\boldsymbol{m})\cdot\hat{\boldsymbol{k}} - \frac{\boldsymbol{r_c}\times\nabla p}{\rho}\cdot\hat{\boldsymbol{k}} + (\boldsymbol{r_c}\times\boldsymbol{g})\cdot\hat{\boldsymbol{k}} + \frac{\boldsymbol{r_c}\times\mathscr{F}}{\rho}\cdot\hat{\boldsymbol{k}}\right],\end{aligned} \tag{2.14}$$

† Note: $\boldsymbol{\Omega}\times\boldsymbol{r} = \boldsymbol{\Omega}\times\boldsymbol{r}_\perp$ together with $\boldsymbol{A}\times(\boldsymbol{B}\times\boldsymbol{C}) = (\boldsymbol{A}\cdot\boldsymbol{C})\boldsymbol{B} - (\boldsymbol{A}\cdot\boldsymbol{B})\boldsymbol{C}$ allow us to write the planetary angular momentum as $\boldsymbol{m_\Omega} = |\boldsymbol{r}_\perp|^2\boldsymbol{\Omega} - |\boldsymbol{r}_{||}||\boldsymbol{\Omega}|\boldsymbol{r}_\perp$.

‡ Egger (2001) did not demonstrate this vector cancellation and led him to conclude that angular momentum conservation was different in the f plane approximation than on the spheroid (in the limit of small aspect ratio $\delta = |ds|/R_e$). We disagree with this statement for the reasons stated above, although we acknowledge Egger (2001) was principally concerned with the β plane approximation.

where we emphasize that $\boldsymbol{r_c}$ is the position vector in the cylindrical coordinate system and $\boldsymbol{g}$ is directed anti-parallel to the unit vector $\hat{\boldsymbol{k}}$ (Figure 4).

Equation 2.14 states that the scalar Lq is conserved following fluid parcels on the f plane if, for non-zero L and q, all of the following conditions are met:

(i) density is conserved ($\Psi = 0$)

(ii) the fluid is inviscid ($\mathscr{F} = 0$)

(iii) the fluid is barotropic ($\nabla\rho \times \nabla p = 0$) **or** the fluid is baroclinic ($\nabla\rho \times \nabla p \neq 0$) and λ is chosen to be a "thermodynamic variable"

(iv) relative angular momentum $\boldsymbol{m}$ is directed vertically so that $(\boldsymbol{\Omega_o} \times \boldsymbol{m}) \cdot \hat{\boldsymbol{k}} = 0$

(v) pressure torques are zero or orthogonal to the vertical so that $(\boldsymbol{r_c} \times \nabla p) \cdot \hat{\boldsymbol{k}} = 0$

(vi) perturbations in Earth's gravitational field are zero so that $(\boldsymbol{r_c} \times \boldsymbol{g}) \cdot \hat{\boldsymbol{k}} = 0$, and

While this equation may find reduced application when compared to Ertel's PV theorem, several simplifications are possible. For inviscid, adiabatic baroclinic flows, selecting λ as proportional to density (*e.g.* $\lambda = -\rho g$) satisfies conditions (i)-(iii). For geophysical flows of the type considered here, the flow is nearly two-dimensional such that $\boldsymbol{m}$ points approximately vertically and condition (iv) is met. For azimuthally symmetric flow away from boundaries pressure gradient torques are zero, so that (v) is satisfied. (Undulating bottom topography will introduce pressure torques.) Finally, in the absence of geopotential perturbations, the sixth term is zero. In conclusion, we have a vorticity theorem valid on the f plane but different than Ertel's PV theorem and yet, at least in highly curved flows away from boundaries, has the potential to satisfy all of the aforementioned conditions. *If these conditions are met, the product of the vertical component of absolute angular momentum and Ertel PV (Lq) is conserved following fluid parcels.*

3. Discussion

It is not clear how best to refer to the quantity Lq. We were at first tempted to refer to this quantity as the generalized potential vorticity since fluid parcels have possible vorticity values set by the sign of Lq through the stability discriminant $\Phi = 2Lq/r^2$ (Buckingham *et al.* 2020*a*,*b*). However, the validity of the theorem is restricted to small horizontal scales such that Lq is not universally conserved. For this reason, *submesoscale potential vorticity* is a suitable alternative.† However, to avoid conflict with the Ertel PV and given its relationship to angular momentum (Rayleigh 1917; Solberg 1936; Fjortoft 1950), we adopt the term *potential momentum* below (denoting it as $\Pi = Lq$), in order to reflect that changes in angular momentum (or curvature) can occur as a result of alterations in the baroclinic nature of the fluid.

Given the restriction to the f plane and our interest in the oceans, the conservation theorem will find greatest application in understanding vortex flows at mid-to-high-latitudes in the oceanic submesoscale regime. Here, we have in mind curved fronts and vortices found at hydrothermal vents and convective plumes (Helfrich & Battisti 1991; D'Asaro *et al.* 1994; Legg & McWilliams 2001; Deremble 2016), within mid-latitude vortices (McDowell & Rossby 1978; McWilliams 1985; Riser *et al.* 1986; Bane *et al.* 1989; Konstianoy & Belkin 1989; Lilly & Rhines 2002; Bosse *et al.* 2016; Meunier *et al.* 2018), and polar mesoscale vortices (D'Asaro 1988; Timmermans *et al.* 2008; Zhao *et al.* 2014). The theorem may also aid in better understanding laboratory vortex flows (Stegner *et al.* 2004; Kloosterziel *et al.* 2007; Lazar *et al.* 2013) and parcel motion within highly curved fronts in the upper ocean

† The scalar $\Phi/f = 2Lq/(fr^2) = (1 + \mathrm{Cu})q$ is perhaps a better variable to be named "submesoscale potential vorticity" since it shares the same units as q and applies to straight and curved fronts. One recovers the Ertel PV in the limit $\mathrm{Cu} \to 0$.

(M. Freilich 2020, personal communication). Such examples are frequently found in strong boundary currents (*e.g.* Gulf Stream and Kuroshio) and the Southern Ocean.

While presenting a framework for understanding sources and sinks of "potential momentum" (Haynes & McIntyre 1987, 1990; Marshall & Nurser 1992) is beyond the scope of this study, one can nevertheless conceptually consider the theorem's application to the aforementioned flows by expressing Equation 2.14 for an axisymmetric vortex flow. This is done below, followed by a discussion of the conservation principle's imprint on vorticity.

3.1. *Axisymmetric vortex flow*

We consider an axisymmetric vortex flow set at high latitudes in cyclogeostrophic and hydrostatic balance (*i.e.* GWB). We assume the flow is located in shallow waters ($|z| < 100$ m). Examples can be found in the halocline eddies observed in the Arctic (Timmermans *et al.* 2008) but we could equally consider application to highly curved fronts in this region (MacKinnon *et al.* 2021). Frictional and diabatic effects are weak such that this balance holds (Eliassen 1951). Formally, we state that deviations from the balanced state are small such that $\boldsymbol{u} = \overline{\boldsymbol{u}} + \boldsymbol{u}^* \approx (0, \overline{v}, 0)$ and $b = \overline{b} + b^* \approx \overline{b}$, where the overbar denotes mean quantities and asterisks (*) denote perturbations from this state. We neglect compressibility, make the Boussinesq approximation, and define $\lambda = -g\rho$, allowing the Ertel PV to be written as $q = \boldsymbol{\omega_a} \cdot \nabla b$, where $b = -g\rho/\rho_o$ is buoyancy and ρ_o is a constant reference density. Finally, we set the meridional component of Coriolis to zero given its distance from the Equator.

We now express Equation 2.14 in cylindrical coordinates. The vertical component of absolute angular momentum is $L = \boldsymbol{m_a} \cdot \hat{\boldsymbol{k}} = (\boldsymbol{m} + \boldsymbol{m_\Omega}) \cdot \hat{\boldsymbol{k}}$, where $\boldsymbol{m} = \boldsymbol{r_c} \times \boldsymbol{u}$ and $\boldsymbol{m_\Omega} = \boldsymbol{r_c} \times (\boldsymbol{\Omega} \times \boldsymbol{r_c})$ are the relative and planetary angular momentum. Together with $\boldsymbol{r_c} = (r, \phi, z)$, $\boldsymbol{u} = (u, v, w)$, and $\boldsymbol{\Omega} = (0, 0, f)$, we find $L = r\overline{v} + fr^2/2$. The Ertel PV for this vortex is $q = (2\boldsymbol{\Omega} + \nabla \times \boldsymbol{u}) \cdot \nabla b$. Together with GWB $(f + 2\overline{v}/r)\partial_z \overline{v} = \partial_r \overline{b} = M^2$, we have $q = (f + \overline{\zeta})N^2 - (f + 2\overline{v}/r)|\partial_z \overline{v}|^2$, where we have neglected the horizontal vorticity owing to its smallness relative to other terms. The relative vorticity associated with the balanced state is $\overline{\zeta} = (1/r)\partial_r(r\overline{v}) = \overline{v}/r + \partial_r \overline{v}$ and vertical stratification is $N^2 = \partial_z \overline{b}$. With these definitions in hand, Equation 2.14 becomes

$$\frac{D\Pi}{Dt} = S_{\mathscr{F}+\mathscr{D}+\mathscr{P}+\mathscr{G}+\Omega}, \tag{3.1}$$

where the potential momentum is

$$\Pi = Lq = \left(r\overline{v} + \frac{fr^2}{2}\right)\left[\left(f + \overline{\zeta}\right)N^2 - \left(f + \frac{2\overline{v}}{r}\right)|\partial_z \overline{v}|^2\right] = \frac{r^2\Phi}{2} \tag{3.2}$$

and $S_{\mathscr{F}+\mathscr{D}+\mathscr{P}+\mathscr{G}+\Omega}$ represents sources and sinks of momentum due to frictional, diabatic, pressure, and gravitational sources, as well as Earth's rotation acting on the relative momentum (*i.e.* RHS of Equation 2.14). Note: Φ is the generalized Rayleigh discriminant and consists of barotropic and baroclinic components (Yim *et al.* 2019; Buckingham *et al.* 2020*a*):

$$\Phi = (f + 2\overline{v}/r)(f + \overline{\zeta})N^2 - (f + 2\overline{v}/r)^2|\partial_z \overline{v}|^2 = \underbrace{\chi^2 N^2}_{barotropic} - \underbrace{M^4}_{baroclinic}, \tag{3.3}$$

where $\chi^2 = (f + 2\overline{v}/r)(f + \overline{\zeta})$ is the generalized Rayleigh discriminant for barotropic vortices (Kloosterziel & van Heijst 1991; Mutabazi *et al.* 1992). We can define non-dimensional gradient Rossby, gradient Richardson, and curvature numbers as $Ro = \overline{\zeta}/f$,

$Ri = N^2/|\partial_z \overline{v}|^2$, and $Cu = 2\overline{v}/fr$, allowing us to also write the potential momentum as

$$\Pi = Lq = \left(\frac{f^2 N^2 r^2}{2}\right)\Phi', \tag{3.4}$$

where

$$\Phi' = L'q' = (1 + Cu)\,(1 + Ro) - (1 + Cu)^2 \cdot Ri^{-1}. \tag{3.5}$$

is a nondimensional form of the Rayleigh discriminant, and $L' = 1 + Cu$ and q' denote nondimensional forms of L and q, respectively. Expanding Equation 3.1, we find

$$\frac{D\Phi}{Dt} = 2S_{\mathscr{F}+\mathscr{D}+\mathscr{P}+\mathscr{Q}+\Omega} - \frac{2u}{r}\Phi. \tag{3.6}$$

In the absence of sources and sinks of potential momentum ($S_{\mathscr{F}+\mathscr{D}+\mathscr{P}+\mathscr{Q}+\Omega} = 0$) and assuming no cross-frontal motion ($u = 0$), the stability of the flow is constant: $D\Phi/Dt = 0$. However, if a fluid parcel moves radially ($u \neq 0$)–even in the absence of sources and sinks of potential momentum–there must be a corresponding change in the stability of the flow.

We now make a clarifying comment. It was previously suggested that the theorem may find utility in understanding parcel motion at curved baroclinic fronts. As a fluid parcel is advected along its path in a meandering flow, we generally expect cross-frontal motion (Bower 1989; Samelson 1992). However, as evidenced by Equation 3.6, Φ is not conserved. Moreover, $D\Phi/Dt = 0$ does not imply $D\Phi'/Dt = 0$, except if N^2 and r^2 do not change following a fluid parcel (cf. Equation 3.4). These conditions can be met within the axisymmetric vortex ($\partial_\phi \overline{b} \approx 0$ and $u \approx 0$) but will not generally be met following fluid parcels within a meandering front. These points therefore clarify statements made by Buckingham *et al.* (2020*a*,*b*).

3.1.1. *A special case:* $S_{\mathscr{F}+\mathscr{D}+\mathscr{P}+\mathscr{Q}+\Omega} = 0$

One of the consequences of Equation 2.14 is that geophysical vortices which reside away from boundaries and perturbations in Earth's geopotential approximately conserve the product of L and q. In the absence of sources and sinks of potential momentum ($S_{\mathscr{F}+\mathscr{D}+\mathscr{P}+\mathscr{Q}+\Omega} = 0$), we can safely approximate cross-frontal motion within an axisymmetric vortex as zero ($u \approx 0$). By virtue of Equation 3.6, this also implies that the Rayleigh discriminant Φ is conserved: $D\Phi/Dt \approx 0$. To understand the consequences of these statements, we consider the evolution of small-scale baroclinic vortices discussed by Buckingham *et al.* (2020*b*).

While the details of this evolution remain unclear without corroborating model support, the following arguments are reasonable. Small-scale baroclinic vortices (radii of 1-10 km) are typically generated in proximity to ocean boundaries due to horizontal shear, baroclinic instability, and convection (Barkley 1972; Legg & McWilliams 2001; Eldevik & Dysthe 2002; Boccaletti *et al.* 2007; Stegner 2014; Bosse *et al.* 2016; Gula *et al.* 2016; MacKinnon *et al.* 2019; Srinivasan *et al.* 2019; Wenegrat *et al.* 2018). These boundaries include the ocean surface, bottom boundary, and ice-ocean boundary. Immediately following formation, they undergo a form of cyclogeostrophic adjustment (Stegner *et al.* 2004), trapping and carrying with them water properties reflective of the boundary layers in which they were formed.

Boundary layer fluid is often characterized by reduced stratification such that, in the presence of vertical shears, $Ri \sim 1$. If this fluid is trapped within the vortex core, then the fluid with low Ri will persist even as the vortex subducts or is advected away from the boundary. One measure of this trapping is the metric $\overline{v}/c$, where $\overline{v}$ is the azimuthal velocity and c is the translation speed of the vortex (Samelson 1992). It follows that the results from Buckingham *et al.* (2020*b*) apply. That is, symmetric instability will be active within cyclonic vortices, while anticyclonic vortices will remain marginally stable, decaying over longer time

scales due to weak inertial-symmetric instabilities.† If the vortex is advected into a different environment, the vortex must alter barotropic and baroclinic components of Φ so as to keep Φ constant. Thus, stratification, shear, and centripetal accelerations (cf. Equation 3.3) must change. In non-dimensional form (cf. Equations 3.4 and 3.5), we see that Ro, Ri, and Cu must change in concert so as to conserve $\Pi = Lq$. Note: Equation 3.4 applies but $D/Dt(N^2) \neq 0$.

3.2. *Revisiting the distribution of relative vorticity*

We return to the joint PDF of vorticity and strain rate observed near the Gulf Stream (Figure 1). We previously noted that as vorticity increased in the cyclonic direction, the joint PDF approached a pure shear relationship, indicative of straight fronts. In contrast, the vorticity was bounded as vorticity decreased toward the negative direction, and a higher probability of vortex flow. While the unbounded nature of cyclonic vorticity associated with straight fronts can be rationalized in terms of PV conservation (Hoskins & Bretherton 1972)‡, the higher probability of anticyclonic vorticity associated with vortex flow has not been explained.

Requiring $Lq > 0$ for all time requires $\Phi > 0$ for all time since $Lq = r^2\Phi/2$. In this case, $D/Dt(Lq) = 0$ *together with an initial positive state* $Lq > 0$ *places constraints on the sign of* Φ *and determines the distribution of relative vorticity in the oceans.* This is analogous to how $Dq/Dt = 0$ together with an initial positive state $fq > 0$ determines the distribution of relative vorticity at straight fronts (Buckingham *et al.* 2016). Another way to state this is that the statistics of vorticity are determined by the possible set of Rossby numbers which ensure the stability discriminant is positive: $\Phi > 0$ or $\Phi' > 0$. If one requires that Equation 3.3 or 3.5 be positive and solves for the set of Rossby numbers which ensure this is true, the negative skewness discussed above will emerge at low Ri (Buckingham *et al.* 2020*b*).

Figure 5 displays $\Phi' = L'q'$ (cf. Equation 3.5) for a range of Richardson, Rossby, and curvature numbers characteristic of a Gaussian vortex in the upper ocean. For clarity, we identify regions of centrifugal and symmetric instability. While Φ' is locally evaluated (here, at the radius of maximum velocity r_m) and cannot describe the global stability of a vortex flow, this nonetheless demonstrates an important point: centripetal accelerations or curvature can shape the distribution of Ro. In particular, for $Ri = 1.0$, anticyclonic flow is (weakly) stable while cyclonic flow is significantly unstable. We therefore expect to see a greater occurrence of anticyclonic vortex flow at $Ri \sim 1$. This is remarkably different than if the front were geostrophic, which predicts cyclonic flow: $Ro > -1 + Ri^{-1}$, or $Ro > 0$.

We now demonstrate this analytically. Introducing a non-dimensional parameter $\mu = Cu/Ro$, which is independent of depth and positive definite within the vortex core ($0 < r < r_m$), and examining solutions for $Ri < \mu$ subject to $\Phi' > 0$, one finds that vorticity Ro principally resides between two curves in dimensionless space, or marginal stability curves (Buckingham *et al.* 2020*b*): $Ro_0 = -\mu^{-1}$ (barotropic root) and $Ro_1 = -(Ri - 1)/(Ri - \mu)$ (baroclinic root). The barotropic root corresponds to the threshold for centrifugal instability ($Cu = -1$), while the baroclinic root corresponds to the threshold for symmetric instability. Selecting $Ri = 1$, one finds that gradient Rossby numbers lie between $-\mu^{-1}$ and 0. Arbitrarily choosing $\mu = 2.0$ (characteristic of Gaussian vortices at

† A timescale for the decay of the cyclonic vortex can be estimated from the growth rate of symmetric disturbances: $T = 2\pi/\sigma$, where $\sigma = f(-\Phi')^{1/2}$ is an approximate growth rate of symmetric disturbances under a simplified axisymmetric vortex model (Buckingham *et al.* 2020*a*, Appendix A). Mahdinia *et al.* (2017) document a decay timescale greater than 50 eddy "turnaround times" for the anticyclonic vortex.

‡ Assuming an initially positive state $fq > 0$, $Dq/Dt = 0$ requires that fq remain positive for all future states. For geostrophic flow and positive stratification, $fq > 0$ can also be written in terms of gradient Rossby and Richardson numbers: $1 + Ro - Ri^{-1} > 0$. Since $Ri > 0$, it follows that Ro is unbounded in the cyclonic direction: $Ro > -1 + Ri^{-1}$.

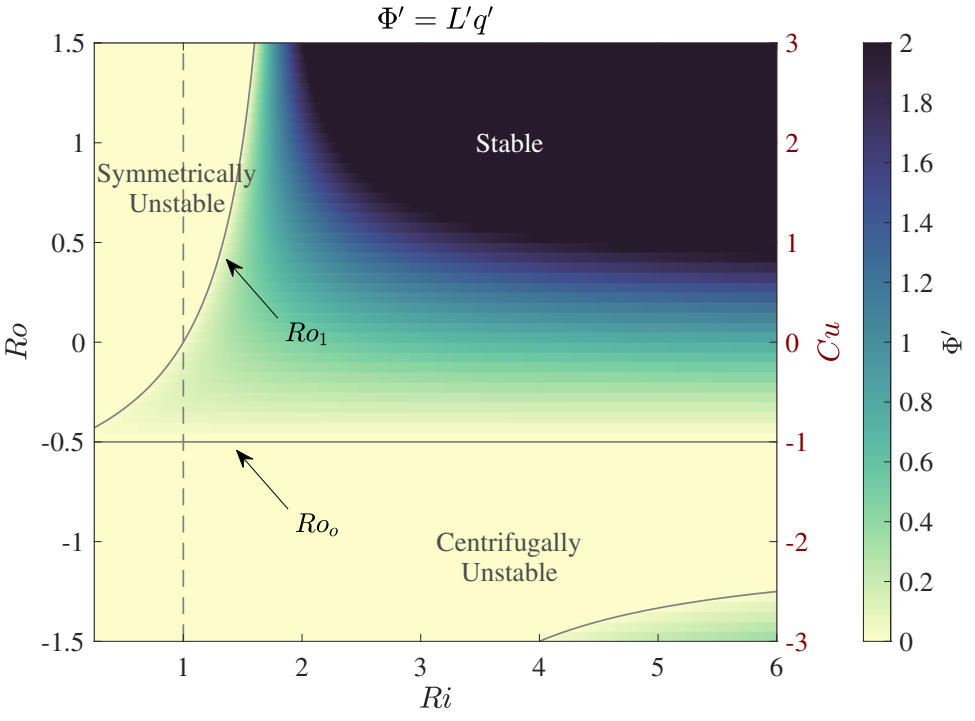

Figure 5: Stability discriminant $\Phi' = L'q'$ as a function of Ro, Ri, and Cu. Observed flows in which Lq is conserved are expected to reside within the stable region $\Phi' > 0$ (blue). This region is delineated from the unstable region (white) by the roots Ro_0 and Ro_1 of Φ' when expressed in terms of the ratio μ (see text). These roots correspond to thresholds for centrifugal and symmetric instability, respectively. For $Ri = 1$ (vertical dashed line), we observe only (weakly) stable anticyclonic flow. This is remarkably different than if the front were geostrophic, which predicts only cyclonic flow (not shown). The stable region in the bottom right corner corresponds to intense, stratified anticyclones for which $\Phi' > 0$, despite that L' and q' are both negative. Such a situation might occur as a result of flow past topography. This graphic is characteristic of Gaussian vortices at the radius of maximum velocity $r = r_m$ (*i.e.* valid for $\mu = 2$).

$r = r_m$) gives $-0.5 < Ro < 0$. That is, the vorticity must be anticyclonic if Lq is conserved. Mahdinia *et al.* (2017) find similar constraints on anticyclonic vortices in their numerical investigation of the stability of three-dimensional Gaussian vortices.

4. Limitations

Our derivation makes the f plane approximation and therefore is restricted to small horizontal scales. Additionally, we isolated the vertical component of absolute angular momentum. As a result, Equation 2.14 cannot be used predict Lq except at the poles since L is coupled to the other components of $\boldsymbol{m_a}$ through $\boldsymbol{\Omega} \times \boldsymbol{m}$. As stated above, this term arises from Earth's rotation and tilts the absolute angular momentum vector away from the vertical, reducing L. This torque is greatest at the Equator and zero at the poles. This does not make Equation 2.14 incorrect but simply limits its utility in certain cases. In summary, the two main limitations to the theory are (i) restriction to the f plane and (ii) reduced applicability in the tropics. These are important limitations since intense frontal flows are frequently found near the Equator (Marchesiello *et al.* 2011; Holmes *et al.* 2013; Simoes-Sousa *et al.* 2021). Progress in this area might be made by examining the recent work of Kloosterziel *et al.* (2017).

It may be worth noting that the f plane approximation together with angular momentum conservation principles have previously been successful for investigating tropical cyclone dynamics (Houze 1993), indicating that these limitations–which grow for vortices closer to the Equator–may not be so severe. It is probable that a more elegant intersection of these three principles will be presented in the future (*i.e.* Figure 2 but where L is replaced by $\boldsymbol{m_a}$).

5. Conclusions

In this study, we have presented a vorticity equation valid on the f plane. It is an extension of Ertel's PV theorem to vortex flow at small horizontal scales such that absolute angular momentum can properly be defined. This leads to a non-trivial result: the combination of absolute angular momentum conservation together with Ertel's theorem has implications for the motion of fluid parcels. In particular, two important consequences of the theorem are (1) stratification, shear, and centripetal accelerations are modified in concert in an effort to conserve Lq and (2) modification to the distribution of relative vorticity opposite to that predicted by geostrophic theory, permitting the occurrence of stable anticyclonic flow, while limiting the occurrences of cyclonic flow at low Richardson numbers. That is, if $Lq > 0$ initially, then $D/Dt(Lq) = 0$ has important consequences for the range of vorticity values seen at small horizontal scales in the ocean. While this may find obvious application in explaining why submesoscale vortices are overwhelmingly anticyclonic, the theorem will also find use in understanding Lagrangian motion within highly curved baroclinic fronts. Given that our present theory of submesoscale flows assumes the mean state to be in geostrophic balance (Thomas *et al.* 2008; McWilliams 2016), the inclusion of centripetal accelerations at the submesoscale represents a shift in direction for the oceanographic community.

The topic of absolute angular momentum conservation has received little attention in oceanography texts, while this same topic has received considerable attention in the atmospheric literature (Holton 1992; Peixoto & Oort 1992; Barnes *et al.* 1983; Bell 1994). This appears to be due to the presence of continental boundaries in the ocean but which are absent in the atmosphere (Griffies 2004), causing PV rather than absolute angular momentum to be a more universally conserved quantity at large horizontal scales (Pedlosky 1987). An exception may be in the Southern Ocean, where obstacles to zonal flow are absent (Straub 1993). However, for small-scale geophysical flows in which centripetal accelerations are present and Earth's rotation plays a dynamically important role,† the conservation of absolute angular momentum finds its place. Submesoscale and polar mesoscale flows are ideal examples in which such a conservation principle may apply. It is in the context of these phenomena that the combined theorem should find greater use.

Acknowledgements. This study was initially made possible by an Individual Fellowship from the European Commission on centrifugal instability (2019-2020). The derivation was made in a two-month period following the fellowship. The author would like to acknowledge the following individuals for helpful conversations (in chronological order): George Nurser, Guillaume Roullet, Keith Nicholls, Greace Crystle, Charly DeMarez, Thomas Meunier, Stephen Griffies, Bruno Deremble, and Amit Tandon.

Declaration of interests. The authors report no conflict of interest.

Data availability statement. No data were used in this study.

† Earth's rotation imparts angular momentum to fluid parcels and can limit centripetal accelerations present in anticyclonic flow through the constraint, $L' = 1 + Cu > 0$, assuming $Cu > -1$ initially. This is analogous to how Earth's rotation imparts vorticity to fluid parcels and limits horizontal shear present in anticyclonic barotropic flow through the constraint, $1 + Ro > 0$.

REFERENCES

Adams, Katherine A., Hosegood, Philip, Taylor, John R., Sallée, Jean-Baptiste, Bachman, Scott, Torres, Ricardo & Stamper, Megan 2017 Frontal circulation and submesoscale variability during the formation of a Southern Ocean mesoscale eddy. *Journal of Physical Oceanography* **47** (7), 1737–1753.

Bane, J. M., O'Keefe, L. M., Watts, D. R., Nihoul, J. C. J. & Jamart, B. M. 1989 *Mesoscale Eddies and Submesoscale, Coherent Vortices: Their Existence Near and Interactions with the Gulf Stream*, *Elsevier Oceanography Series*, vol. 50, pp. 501–518. Elsevier.

Barkley, Richard A. 1972 Johnston Atoll's wake. *Journal of Marine Research* **30** (2), 201–216.

Barnes, R. T. H., Hide, Raymond, White, A. A. & Wilson, C. A. 1983 Atmospheric angular momentum fluctuations, length-of-day changes and polar motion. *Proceedings of the Royal Society of London. A. Mathematical and Physical Sciences* **387** (1792), 31–73.

Batchelor, G. K. 1967 *An Introduction to Fluid Dynamics*. Cambridge: Cambridge University Press.

Bell, M. J. 1994 Oscillations in the equatorial components of the atmosphere's angular momentum and torques on the Earth's bulge. *Quarterly Journal of the Royal Meteorological Society* **120** (515), 195–213.

Boccaletti, Giulio, Ferrari, Raffaele & Fox-Kemper, Baylor 2007 Mixed layer instabilities and restratification. *Journal of Physical Oceanography* **37** (9), 2228–2250.

Bosse, Anthony, Testor, Pierre, Houpert, Lo ic, Damien, Pierre, Prieur, Louis, Hayes, Daniel, Taillandier, Vincent, Durrieu de Madron, Xavier, d'Ortenzio, Fabrizio, Coppola, Laurent, Karstensen, Johannes & Mortier, Laurent 2016 Scales and dynamics of submesoscale coherent vortices formed by deep convection in the northwestern Mediterranean Sea. *Journal of Geophysical Research: Oceans* **121** (10), 7716–7742.

Bower, Amy S. 1989 Potential vorticity balances and horizontal divergence along particle trajectories in Gulf Stream meanders east of Cape Hatteras. *Journal of Physical Oceanography* **19** (11), 1669–1681.

Buckingham, Christian E., Gula, Jonathan & Carton, Xavier 2020*a* The role of curvature in modifying frontal instabilities, part 1. *Journal of Physical Oceanography* .

Buckingham, Christian E., Gula, Jonathan & Carton, Xavier 2020*b* The role of curvature in modifying frontal instabilities, part 2. *Journal of Physical Oceanography* .

Buckingham, Christian E., Naveira Garabato, Alberto C., Thompson, Andrew F., Brannigan, Liam, Lazar, Ayah, Marshall, David P., George Nurser, A. J., Damerell, Gillian, Heywood, Karen J. & Belcher, Stephen E. 2016 Seasonality of submesoscale flows in the ocean surface boundary layer. *Geophys. Res. Lett.* **43**, 2118–2126, 2016GL068009.

Chelton, Dudley B., deSzoeke, Roland A., Schlax, Michael G., El Naggar, Karim & Siwertz, Nicolas 1998 Geographical variability of the first baroclinic rossby radius of deformation. *Journal of Physical Oceanography* **28** (3), 433–460.

Cushman-Roisin, Benoit 1994 *Introduction to Geophysical Fluid Dynamics*. Englewood Cliffs, N.J.: Prentice Hall.

D'Asaro, Eric, Lee, Craig, Rainville, Luc, Harcourt, Ramsey & Thomas, Leif 2011 Enhanced turbulence and energy dissipation at ocean fronts. *Science* **332** (6027), 318–322.

D'Asaro, Eric, Walker, Sharon & Baker, Edward 1994 Structure of two hydrothermal megaplumes. *Journal of Geophysical Research: Oceans* **99** (C10), 20361–20373.

D'Asaro, Eric A. 1988 Observations of small eddies in the Beaufort Sea. *Journal of Geophysical Research: Oceans* **93** (C6), 6669–6684.

Deremble, Bruno 2016 Convective plumes in rotating systems. *Journal of Fluid Mechanics* **799**, 27–55.

Egger, Joseph 2001 Angular momentum of β-plane flows. *Journal of the Atmospheric Sciences* **58** (17), 2502–2508.

Eldevik, Tor & Dysthe, Kristian B. 2002 Spiral eddies. *Journal of Physical Oceanography* **32** (3), 851–869.

Eliassen, Arnt 1951 Slow thermally or frictionally controlled meridional circulation in a circular vortex. *Astrophysica Norvegica* **5** (2), 1–42.

Ertel, Hans 1942 Ein neuer hydrodynamischer wirbelsatz. *Meteorol. Z.* **59**, 271–281.

Fjortoft, R. 1950 Application of integral theorems in deriving criteria of stability for laminar flows and for the baroclinic circular vortex. *Geophys. Publ.* **17** (6), 1–52.

Flament, Pierre, Armi, Laurence & Washburn, Libe 1985 The evolving structure of an upwelling filament. *Journal of Geophysical Research: Oceans* **90** (C6), 11765–11778.

Gentemann, C. L., Scott, Joel P., Mazzini, Piero L. F., Pianca, Cassia, Akella, Santha, Minnett,

Peter J., Cornillon, Peter, Fox-Kemper, Baylor, Cetinić, Ivona, Chin, T. Mike, Gomez-Valdes, Jose, Vazquez-Cuervo, Jorge, Tsontos, Vardis, Yu, Lisan, Jenkins, Richard, Halleux, Sebastien De, Peacock, Dave & Cohen, Nora 2020 Saildrone: Adaptively sampling the marine environment. *Bulletin of the American Meteorological Society* **101** (6), E744–E762.

Griffies, Stephen M. 2004 *Fundamentals of Ocean Climate Models*. Princeton: Princeton University Press.

Grimshaw, R. H. J. 1975 A note on the β-plane approximation. *Tellus* **27** (4), 351–357.

Gula, Jonathan, Molemaker, M. Jeroen & McWilliams, James C. 2016 Topographic generation of submesoscale centrifugal instability and energy dissipation. *Nature Communications* **7**.

Haynes, P. H. & McIntyre, M. E. 1987 On the evolution of vorticity and potential vorticity in the presence of diabatic heating and frictional or other forces. *Journal of the Atmospheric Sciences* **44** (5), 828–841.

Haynes, P. H. & McIntyre, M. E. 1990 On the conservation and impermeability theorems for potential vorticity. *Journal of the Atmospheric Sciences* **47** (16), 2021–2031.

Helfrich, Karl R. & Battisti, Thomas M. 1991 Experiments on baroclinic vortex shedding from hydrothermal plumes. *Journal of Geophysical Research: Oceans* **96** (C7), 12511–12518.

Holmes, Ryan M., Thomas, Leif N., Thompson, LuAnne & Darr, David 2013 Potential vorticity dynamics of tropical instability vortices. *Journal of Physical Oceanography* **44** (3), 995–1011.

Holton, James R. 1992 *An Introduction to Dynamic Meteorology*, 3rd edn. Academic Press.

Hoskins, B. J. & Bretherton, F. P. 1972 Atmospheric frontogenesis models: mathematical formulation and solution. *Journal of the Atmospheric Sciences* **29**, 11–37.

Houze, R. 1993 *Cloud dynamics*, *International Geophysics Series*, vol. 53. Academic Press.

Kloosterziel, R. C., Carnevale, G. F. & Orlandi, P. 2007 Inertial instability in rotating and stratified fluids: barotropic vortices. *Journal of Fluid Mechanics* **583**, 379–412.

Kloosterziel, R. C., Carnevale, G. F. & Orlandi, P. 2017 Equatorial inertial instability with full Coriolis force. *Journal of Fluid Mechanics* **825**, 69–108.

Kloosterziel, R. C. & van Heijst, G. J. F. 1991 An experimental study of unstable barotropic vortices in a rotating fluid. *Journal of Fluid Mechanics* **223**, 1–24.

Konstianoy, Andrey G. & Belkin, I. M. 1989 *A survey of observations on intrathermocline eddies in the world ocean*, pp. 821–841. Elsevier Academic Press.

Lazar, Ayah, Stegner, A., Caldeira, R., Dong, C., Didelle, H. & Viboud, S. 2013 Inertial instability of intense stratified anticyclones. part 2. laboratory experiments. *Journal of Fluid Mechanics* **732**, 485–509.

Legg, Sonya & McWilliams, James C. 2001 Convective modifications of a geostrophic eddy field. *Journal of Physical Oceanography* **31** (4), 874–891.

Lilly, Jonathan M. & Rhines, Peter B. 2002 Coherent eddies in the Labrador Sea observed from a mooring. *Journal of Physical Oceanography* **32**, 585–598.

MacKinnon, Jennifer A., Alford, Matthew H., Voet, Gunnar, Zeiden, Kristin L., Shaun Johnston, T. M., Siegelman, Mika, Merrifield, Sophia & Merrifield, Mark 2019 Eddy wake generation from broadband currents near Palau. *Journal of Geophysical Research: Oceans* **124** (7), 4891–4903.

MacKinnon, Jennifer A., Simmons, Harper L., Hargrove, John, Thomson, Jim, Peacock, Thomas, Alford, Matthew H., Barton, Benjamin I., Boury, Samuel, Brenner, Samuel D., Couto, Nicole, Danielson, Seth L., Fine, Elizabeth C., Graber, Hans C., Guthrie, John, Hopkins, Joanne E., Jayne, Steven R., Jeon, Chanhyung, Klenz, Thilo, Lee, Craig M., Lenn, Yueng-Djern, Lucas, Andrew J., Lund, Björn, Mahaffey, Claire, Norman, Louisa, Rainville, Luc, Smith, Madison M., Thomas, Leif N., Torres-Valdés, Sinhué & Wood, Kevin R. 2021 A warm jet in a cold ocean. *Nature Communications* **12** (1), 2418.

Mahdinia, Mani, Hassanzadeh, Pedram, Marcus, Philip S. & Jiang, Chung-Hsiang 2017 Stability of three-dimensional Gaussian vortices in an unbounded, rotating, vertically stratified, Boussinesq flow: linear analysis. *Journal of Fluid Mechanics* **824**, 97–134.

Marchesiello, Patrick, Capet, Xavier, Menkes, Christophe & Kennan, Sean C. 2011 Submesoscale dynamics in tropical instability waves. *Ocean Modelling* **39** (1), 31–46.

Marshall, John C. & Nurser, A. J. George 1992 Fluid dynamics of oceanic thermocline ventilation. *Journal of Physical Oceanography* **22** (6), 583–595.

McDowell, Scott E. & Rossby, H. Thomas 1978 Mediterranean water: an intense mesoscale eddy off the bahamas. *Science* **202**, 1085–1087.

McWilliams, James C. 1985 Submesoscale, coherent vortices in the ocean. *Reviews of Geophysics* **23** (2), 165–182.

McWilliams, James C. 2016 Submesoscale currents in the ocean. *Proceedings of the Royal Society of London A: Mathematical, Physical and Engineering Sciences* **472** (2189), 1–32.

Meunier, Thomas, Tenreiro, M., Pallàs-Sanz, Enric, Ochoa, Jose, Ruiz-Angulo, Angel, Portela, Esther, Cusí, Simò, Damien, Pierre & Carton, Xavier 2018 Intrathermocline eddies embedded within an anticyclonic vortex ring. *Geophysical Research Letters* **45** (15), 7624–7633.

Müller, Peter 1995 Ertel's potential vorticity theorem in physical oceanography. *Reviews of Geophysics* **33** (1), 67–97.

Munk, Walter, Armi, Laurence, Fischer, Kenneth & Zachariasen, F 2000 Spirals on the sea. In *Proceedings of the Royal Society of London A: Mathematical, Physical and Engineering Sciences*, , vol. 456, pp. 1217–1280. The Royal Society.

Mutabazi, Innocent, Normand, Christiane & Wesfreid, José Eduardo 1992 Gap size effects on centrifugally and rotationally driven instabilities. *Physics of Fluids A: Fluid Dynamics* **4** (6), 1199–1205.

Naveira Garabato, Alberto C., Frajka-Williams, Eleanor E., Spingys, Carl P., Legg, Sonya, Polzin, Kurt L., Forryan, Alexander, Abrahamsen, E. Povl, Buckingham, Christian E., Griffies, Stephen M., McPhail, Stephen D., Nicholls, Keith W., Thomas, Leif N. & Meredith, Michael P. 2019 Rapid mixing and exchange of deep-ocean waters in an abyssal boundary current. *Proceedings of the National Academy of Sciences* **116** (27), 13233.

Nurser, A. J. George & Bacon, Sheldon 2014 The Rossby radius in the Arctic Ocean. *Ocean Sci.* **10**, 967–975.

Onken, R., Baschek, B. & Angel-Benavides, I. M. 2020 Very high-resolution modelling of submesoscale turbulent patterns and processes in the Baltic Sea. *Ocean Science* **16** (3), 657–684.

Pedlosky, Joseph 1987 *Geophysical Fluid Dynamics*, 2nd edn. New York: Springer New York.

Peixoto, Jose P. & Oort, Abraham H. 1992 *Physics of Climate*, 1st edn. American Institute of Physics Press.

du Plessis, Marcel, Swart, Sebastiaan, Ansorge, Isabelle J., Mahadevan, Amala & Thompson, Andrew F. 2019 Southern Ocean seasonal restratification delayed by submesoscale wind–front interactions. *Journal of Physical Oceanography* **49** (4), 1035–1053.

Rayleigh, Lord 1917 On the dynamics of revolving fluids. *Proc. Royal Society of London. Series A, Containing Papers of a Mathematical and Physical Character* **93**, 148–154.

Riley, K. F., Hobson, M. P. & Bence, S. J. 2006 *Mathematical Methods for Physics and Engineering: A Comprehensive Guide*, 3rd edn. Cambridge: Cambridge University Press.

Riser, Stephen C., Owens, W. Brechner, Rossby, H. Thomas & Ebbesmeyer, Curtis C. 1986 The structure, dynamics, and origin of a small-scale lens of water in the western North Atlantic thermocline. *Journal of Physical Oceanography* **16** (3), 572–590.

Roullet, Guillaume & Klein, Patrice 2010 Cyclone-anticyclone asymmetry in geophysical turbulence. *Physical Review Letters* **104** (21), 1–4.

Rudnick, Daniel L. 2001 On the skewness of vorticity in the upper ocean. *Geophysical Research Letters* **28** (10), 2045–2048.

Samelson, R. M. 1992 Fluid Exchange across a Meandering Jet. *Journal of Physical Oceanography* **22** (4), 431–444.

Scully-Power, Paul 1986 Navy Oceanographer Shuttle observations, STS 41-G Mission Report. *Tech. Rep.*. DTIC Document, Newport, Rhode Island.

Shakespeare, Callum J. 2016 Curved density fronts: Cyclogeostrophic adjustment and frontogenesis. *Journal of Physical Oceanography* **46**, 3193–3207.

Shcherbina, Andrey Y., D'Asaro, Eric A., Lee, Craig M., Klymak, Jody M., Molemaker, M. Jeroen & McWilliams, James C. 2013 Statistics of vertical vorticity, divergence, and strain in a developed submesoscale turbulence field. *Geophysical Research Letters* **40** (17), 4706–4711.

Simoes-Sousa, Iury T., Silveira, Ilson Carlos A., Tandon, Amit, Flierl, Glenn R., Ribeiro, Cesar H. A. & Martins, Renato P. 2021 The Barreirinhas eddies: Stable energetic anticyclones in the near-equatorial South Atlantic. *Frontiers in Marine Science* **8**, 28.

Smith, K. Shafer 2007 The geography of linear baroclinic instability in Earth's oceans. *Journal of Marine Research* **65** (5), 655–683.

Solberg, H. 1936 Le mouvement d'inertie de l'atmosphere stable et son role dans la theorie des cyclones. In *Sixth Assembly*, pp. 66–82. Union Geodesique et Geophysique Internationale, Edinburgh: Paul Dupont.

Srinivasan, Kaushik, McWilliams, James C., Molemaker, M. Jeroen & Barkan, Roy 2019

671 Submesoscale vortical wakes in the lee of topography. *Journal of Physical Oceanography* **49** (7),
672 1949–1971.
673 Stegner, Alexandre 2014 *Oceanic Island Wake Flows in the Laboratory*, chap. 14, pp. 265–276. American
674 Geophysical Union (AGU).
675 Stegner, A., Bouret-Aubertot, P. & Pichon, T. 2004 Nonlinear adjustment of density fronts. Part 1. the
676 Rossby scenario and the experimental reality. *Journal of Fluid Mechanics* **502**, 335–360.
677 Straub, David N. 1993 On the transport and angular momentum balance of channel models of the Antarctic
678 Circumpolar Current. *Journal of Physical Oceanography* **23** (4), 776–782.
679 Thomas, Leif N. & Lee, Craig M. 2005 Intensification of ocean fronts by down-front winds. *J. Phys.*
680 *Oceanogr.* **35**, 1086–1102.
681 Thomas, Leif N, Tandon, Amit & Mahadevan, Amala 2008 Submesoscale processes and dynamics.
682 *Ocean Modeling in an Eddying Regime, Geophys. Monogr. Ser* **177**, 17–38.
683 Thomas, Leif N., Taylor, John R., Ferrari, Raffaele & Joyce, T. M. 2013 Symmetric instability in the
684 Gulf Stream. *Deep Sea Research Part 2* **91**, 91–110.
685 Thompson, Andrew F., Lazar, Ayah, Buckingham, Christian E., Naveira Garabato, Alberto C.,
686 Damerell, Gillian M. & Heywood, Karen J. 2016 Open-ocean submesoscale motions: A full
687 seasonal cycle of mixed layer instabilities from gliders. *J. Phys. Oceanogr.* .
688 Timmermans, M-L., Toole, J., Proshutinsky, A., Krishfield, R. & Plueddemann, A. 2008 Eddies in the
689 Canada Basin, Arctic Ocean, observed from ice-tethered profilers. *Journal of Physical Oceanography*
690 **38** (1), 133–145.
691 Wenegrat, Jacob O., Callies, J orn & Thomas, Leif N. 2018 Submesoscale baroclinic instability in the
692 bottom boundary layer. *Journal of Physical Oceanography* **48** (11), 2571–2592.
693 Yim, Eunok, Stegner, Alexandre & Billant, Paul 2019 Stability criterion for the centrifugal instability
694 of surface intensified anticyclones. *Journal of Physical Oceanography* **49** (3), 827–849.
695 Zhao, Mengnan, Timmermans, Mary-Louise, Cole, Sylvia, Krishfield, Richard, Proshutinsky,
696 Andrey & Toole, John 2014 Characterizing the eddy field in the Arctic Ocean halocline. *Journal*
697 *of Geophysical Research: Oceans* **119** (12), 8800–8817.